Sigma J Eng & Nat Sci 35 (1), 2017, 133-155

Sigma Journal of Engineering and Natural Sciences
Sigma Mühendislik ve Fen Bilimleri Dergisi

Research Article / Araştırma Makalesi

NUMERICAL SIMULATION OF SUBSONIC TURBULENT FLOW OVER NACA0012 AIRFOIL: EVALUATION OF TURBULENCE MODELS

Seyed Mostafa MOUSAVI, Javad AMINIAN*[1], Navvab SHAFIEI[2], Abdolrahman DADVAND[3]

[1]*Faculty of Mechanical and Energy Engineering, Shahid Beheshti University, Tehran, IRAN*
[2]*Department of Engineering, Imam Khomeini International University, Qazvin, IRAN.*
[3]*Department of Mechanical Engineering, Urmia University of Technology, Urmia, IRAN*

Received/Geliş: 02.03.2016 Revised/Düzeltme: 13.10.2016 Accepted/Kabul: 10.01.2017

ABSTRACT

Subsonic turbulent flow over NACA0012 airfoil at the Reynolds number of 3×10^6 and different angles of attack (from -12º to 20º) is simulated using OpenFOAM. The flow is assumed 133ort steady and two-dimensional. Different turbulence models including Spalart-Allmaras, realizable k-ε and k-ω Shear Stress Transport (SST) are employed and their accuracy evaluated through the comparison 133ort h results with the available experimental data. The main focus has been put on the two regions around the airfoil, namely, the transition region and the turbulent region that are of high importance in the evaluation of computational fluid dynamics (CFD) codes. Hence, the laminar to turbulent transition point was determined at various Reynolds numbers in order to get accurate results 133ort he drag coefficient. It was found that by increasing the angle of attack, the accuracy of all the turbulence models used in the OpenFOAM software would reduce. In addition, the Spalart-Allmaras model showed highest accuracy compared with the other models tested in the present research. In fact, these turbulence models are unable to detect the point where the transition from laminar to turbulent flow occurs and thus have deficiency in determining the accurate flow quantities. Therefore, in both the theoretical and empirical studies the transition effects should be taken into account especially in critical analyses.
Keywords: Subsonic, NACA0012 airfoil, turbulence models, transition region, computational fluid dynamics, OpenFOAM.

NACA0012 HAVA FOLYOLARINDA SESALTI DÜZENSİZ AKIŞIN SAYISAL SİMÜLASYONU: TÜRBÜLANS MODELLERİNİN DEĞERLENDİRİLMESİ

ÖZ

NACA0012 hava folyolarında altsonik düzensiz akışı, farklı saldırı açılardan (-12° ila 20° arası) ve Reynolds 3×10^6, OpenFOAM ile simüle edilir. Akış, dinamik ve iki boyutlu olarak kabul edilir. Spalart-Allmaras, Realizable k-ε ve k-Ω Shear Stress Transport (SST) gibi farklı düzensiz modelleri kullanılmış ve her birinin doğruluğu, sonuçların ve mevcut deney verileri ile karşılaştırılarak değerlendirilmiştir.Temel odağı, hava folyosundaki iki akış alanına yani geçiş ve düzensiz noktasında odaklanmıştır, bunlar Hesaplamalı Akışkanlar Dinamiği (HAD) Kodlarının değerlendirilmesinde önem taşınmaktadir. Bu nedenle, sürüklenme katsayısını doğru bir şekilde hesaplamak için, kaygan'dan düzensiz'e geçiş noktası, farklı Reynolds sayılarında belirlenmiştir. Sonuçlar, saldırı açısının artmasıyla OpenFOAM yazılımındaki türbülans modellerinin doğruluğunun azaldığını gösteriyor. Üstelik bu çalışmada, Spalart-Allmaras modeli diğer iki modellerden daha doğru olmuştur. Aslında, bahsedilen türbülans modelleri, kaygan'dan düzensiz'e geçişini tanımayabilmektedir; Bu nedenle, akış miktarlarının belirlenmesinde hatalar oluşur. Dolayısıyla teorik ve deneysel çalışmalarda, özellikle kritik analizlerde, geçiş etkilerinin göz önüne alınmalıdır.
Anahtar Sözcükler: Sesaltı, NACA0012 hava folyoları, türbülans modelleri, geçiş noktası, hesaplamalı akışkan dinamiği, OpenFOAM.

* Corresponding Author/Sorumlu Yazar: e-mail/e-ileti: j_aminian@sbu.ac.ir, tel: (+98 21) 73932693

1. INTRODUCTION

The growing necessity for robust and accurate models to simulate the flows around various industrial equipment and objects has resulted in rapid development and evolution of computational fluid dynamics (CFD) methods. In the past few decades, CFD has been used to design many spacecraft, vehicles and industrial elements and the processes in which the flows of fluids would play an essential role. The complexity of the governing equations, the mutual influence of different physical phenomena, the transient nature of most of engineering problems, the high costs of laboratory equipment and the limitation on using measurement devices in many experimental problems are among the reasons that limit the use of analytical and experimental methods as compared with numerical methods.

Investigation of aerodynamic characteristics of airfoils has significant importance in both external and internal flows. Among the most applications of airfoils one may refer to the designation of lifting surfaces (such as fixed and movable wings and control surfaces of aircrafts, helicopters and missiles), the profiles utilized in the designation and construction of fan, compressor and turbine of air-breathing engines and wind turbines blades [1].

In the simulation of flow around an airfoil, the location where transition from fully laminar flow to fully turbulent flow occurs plays an important role in determination of flow characteristics and airfoil performance including the lift and drag coefficients, the center of pressure, the interaction position between shock and boundary layer, the boundary layer transition position, the flow separation position and the change in pressure and shear stress distribution. Bacha and Ghaly introduced a transition model composed of the existing models to predict the onset and extent of transition [2]. Their model is consistent with the Spalart-Allmaras turbulence model. According to this model, the inception of transition is based on Michel criterion in two-dimensional incompressible flows while the extent of transition is modeled by a periodic function. Johansen addressed the investigation of transition position around the NACA0012 airfoil in incompressible flow at low and moderate Reynolds (Re) numbers and fixed angle of attack [3]. He applied e^N model (linear stability analysis) and Michel criterion and used the changes in the friction drag coefficient and shape factor to predict the transition position around different airfoils.

McCroskey et al. classified and analyzed the results associated with aerodynamic properties of NACA0012 airfoil obtained from the experimental tests performed in more than 40 valid wind tunnels in the world [4]. They also sought and analyzed the error sources in each experiment. They considered a wide range of Re numbers (from several hundreds of thousands to several millions) and Mach numbers (from subsonic to transonic). Therefore, these data could be used for validation purposes with reliable accuracy. Maksymiuk and Pulliam developed a finite difference two-dimensional computational code ARC2D, for fully turbulent viscous flow with zero-equation Baldwin-Lomax turbulence model [5]. Different flow conditions (Mach numbers of 0.5 to 1.1 and different angles of attack) were tested and the aerodynamic coefficients were compared to the valid experimental data. Using finite volume numerical method, Arias et al. analyzed the flow around NACA0012 airfoil for Mach numbers of 0.8 to 1.2 and different angles of attack [6]. The distribution of pressure coefficient and the parameters affecting the convergence of the applied numerical method were investigated. But, due to the use of Euler equations, the performed analyses were fully non-viscous and hence the viscosity effects and boundary layer formation were not captured. Barter used Galerkin finite element method and incorporated artificial viscosity and adaptive mesh refinement to numerically simulate the flow field around NACA0012 airfoil for different Mach numbers ranging from 0.8 to 2 in the transonic and supersonic regimes [7]. In his work, the viscous effects were only accounted for at the Mach number equal to 2. Therefore, the interaction between shock and boundary layer was mainly not addressed.

One of the challenging issues in many CFD packages is that the whole flow domain has to be assumed fully laminar or fully turbulent and hence the transition region is ignored. This would give rise to remarkable errors, which need to be minimized in order to obtain accurate results. Hence, our main purpose in this work is to properly model both the onset and extent of transition by OpenFOAM and to calculate the flow characteristics around the airfoil accurately. This approach not only increases the accuracy of the results, but also reveals the importance and necessity of the consideration of transition region.

In this paper, the dependence of lift and drag coefficients of NACA0012 airfoil on the angle of attack is investigated using three different turbulence models available in free access code OpenFOAM. So far, different turbulence models were introduced each of which has its own feature that is suitable for special cases. Most of these models are not able to detect the position of transition from laminar to turbulent. Therefore, the goal of this research is to examine some of these models and find among them a proper turbulence model, which is able to accurately predict the onset of transition and to evaluate its effects on the drag coefficient. Here, the Spalart-Allmaras model, the realizable k-ε model and the k-ω Shear Stress Transport (SST) model are used to simulate the flow over the classic NACA0012 airfoil. The results are compared with the available experimental data.

2. GOVERNING EQUATIONS FOR TURBULENT FLOW

2.1. RANS (Reynolds-Averaged Navier Stokes) Equations

The RANS equations governing a compressible turbulent flow encompass the continuity, momentum and energy equations and the equation of state [1,8,9]:

$$\frac{\partial \rho}{\partial t} + \frac{\partial}{\partial x_j}\left(\rho u_j\right) = 0 \tag{1}$$

$$\frac{\partial\left(\rho u_j\right)}{\partial t} + \frac{\partial\left(\rho u_i u_j\right)}{\partial x_i} = -\frac{\partial p}{\partial x_j} + \frac{\partial}{\partial x_i}\tau_{ij} + \frac{\partial}{\partial x_i}\left(-\rho\overline{u_i' u_j'}\right) + S_{M_j} \tag{2}$$

$$\frac{\partial\left(\rho E\right)}{\partial t} + \frac{\partial\left(u_j\left(\rho E + p\right)\right)}{\partial x_j} = \frac{\partial}{\partial x_j}\left[\left(\eta + \frac{c_p \mu_t}{\mathrm{Pr}_t}\right)\frac{\partial T}{\partial x_j} + u_i \tau_{ij}\right] \tag{3}$$

$$p = \rho R T \tag{4}$$

The Reynolds stress term $-\rho\overline{u_i' u_j'}$ in the right side of Eq. (2) is related to the velocity gradients by using the Boussinesq approximation [10]. The source term S_{M_j} represents the body forces per unit volume per unit time. In Eq. (3), η is thermal conductivity, E is total energy, $\mathrm{Pr_t}$ is turbulent Prandtl number and τ_{ij} is deviatoric stress tensor expressed in Eq. (5) [8]:

$$\tau_{ij} = \mu\left[\frac{\partial u_i}{\partial x_j} + \frac{\partial u_j}{\partial x_i} - \frac{2}{3}\frac{\partial u_k}{\partial x_k}\delta_{ij}\right] \tag{5}$$

Where μ is the molecular viscosity and δ_{ij} is the Kronecker delta. As the governing system of equations is still not closed (the number of unknowns is more than the number of equations) different turbulence models are used to solve this system of equations. In the present article we examine three of these models, which are more practical for modeling of turbulent flow around an airfoil.

2.2. Boussinesq Approximation

In a turbulence model, the Reynolds stress term $-\rho\overline{u_i'u_j'}$ in the right hand side of Eq. (2) should be modeled. One way to model this term is the Boussinesq approximation, which relates it to the mean flow velocity gradients [10,11]:

$$-\rho\overline{u_i'u_j'} = \mu_t\left(\frac{\partial u_i}{\partial x_j}+\frac{\partial u_j}{\partial x_i}\right)-\frac{2}{3}\left(\rho k+\mu_t\frac{\partial u_j}{\partial x_j}\right)\delta_{ij} \tag{6}$$

Where k is turbulence kinetic energy (the sum of the diagonal components of the Reynolds stress tensor) and μ_t denotes the eddy viscosity.

2.3. Spalart-Allmaras Turbulence Model

Spalart-Allmaras model is a one-equation model that solves a modeled transport equation for the kinematic eddy viscosity (without calculating the length scale of the shear layer thickness). The differential equation is derived by using the empiricism and arguments of dimensional analysis, Galilean invariance and dependence on the molecular viscosity. This model is known for its good results in a wide range of flow problems and its numerical properties [12]. It was developed for aerospace applications and has given good results for the boundary layers exposed to adverse pressure gradient [13]. Also, it has acceptable validity for transonic and supersonic turbulent flow in complex industrial configurations and slightly separated flow in over-expanded nozzles [12,14,15,16]. Spalart-Allmaras model is an effective model for low Reynolds number flows. Therefore, the effective use of this model is limited to the regions within the boundary layer affected by the viscosity. This model compared to the k-ε model is less sensitive to the deflections in the mesh zone (which can lead to the false diffusion). Experience has shown that in flows with reducing velocity and adverse pressure gradient, this model can give better results than the k-ε model.

In Spalart-Allmaras turbulence model, the transport equation for the working variable $\tilde{\nu}$ is represented as bellows [12,13]:

$$\frac{\partial\tilde{\nu}}{\partial t}+u_j\frac{\partial\tilde{\nu}}{\partial x_j}=\underbrace{c_{b1}(1-f_{t2})\tilde{S}\tilde{\nu}}_{\text{Production}}+\underbrace{\frac{1}{\sigma}\left[\frac{\partial}{\partial x_j}\left((\nu+\tilde{\nu})\frac{\partial\tilde{\nu}}{\partial x_j}\right)+c_{b2}\left(\frac{\partial\tilde{\nu}}{\partial x_i}\right)^2\right]}_{\text{Diffusion}} \tag{7}$$
$$-\underbrace{\left[c_{w1}f_w-\frac{c_{b1}}{\kappa^2}f_{t2}\right]\left[\frac{\tilde{\nu}}{d}\right]^2}_{\text{Destruction}}+\underbrace{f_{t1}\Delta U^2}_{\text{Transition}}$$

Where $\nu=\mu/\rho$ is molecular kinematic viscosity, d is distance to the closest wall and ΔU represents the difference between the velocity of a point of field and the velocity of trip (on the wall). Eddy viscosity is given by [12,13,17]:

$$\mu_t=\rho\tilde{\nu}f_{v1}=\rho\nu_t \tag{8}$$

Where f_{v1} is damping function defined as [12]:

$$f_{v1} = \frac{\left(\frac{\tilde{\nu}}{\nu}\right)^3}{\left(\frac{\tilde{\nu}}{\nu}\right)^3 + c_{v1}^3} \tag{9}$$

Also, magnitude of vorticity $\tilde{S}$, f_{t1} and f_{t2} is defined as [13]:

$$\tilde{S} \equiv \sqrt{2\Omega_{ij}\Omega_{ij}} + \frac{\tilde{\nu}}{\kappa^2 d^2}[\arg_1],$$

$$\arg_1 = 1 - \left(\frac{\tilde{\nu}}{\nu}\right)\left[1 + \frac{\left(\frac{\tilde{\nu}}{\nu}\right)^4}{\left[\left(\frac{\tilde{\nu}}{\nu}\right)^3 + c_{v1}^3\right]}\right]^{-1}, \tag{10}$$

$$\Omega_{ij} = \frac{1}{2}\left(\frac{\partial u_i}{\partial x_j} - \frac{\partial u_j}{\partial x_i}\right)$$

$$f_{t1} = c_{t1} g_t \exp(Z),$$

$$Z = -c_{t2}\frac{\omega_t^2}{\Delta U^2}\left(d^2 + g_t^2 d_t^2\right), \tag{11}$$

$$f_{t2} = c_{t3}\exp\left[-c_{t4}\left(\frac{\tilde{\nu}}{\nu}\right)^2\right]$$

In these equations, Ω_{ij} is the rate-of-rotation tensor, d_t is the distance of a point in the flow field to trip on the wall and ω_t is the wall vorticity at the trip point. Also g_t=min(0.1,$\Delta U/\omega_t \Delta x$) where Δx is the grid distance along the wall at the trip. The function f_w is used in order to determine the destruction behavior in outer region of the boundary layer [12]:

$$f_w(g) = g\left(\frac{1 + c_{w3}^6}{g^6 + c_{w3}^6}\right)^{\frac{1}{6}},$$

$$g = r + c_{w2}\left(r^6 - r\right), \tag{12}$$

$$r = \frac{\tilde{\nu}}{\tilde{S}\kappa^2 d^2}$$

r and f_w in the log-layer are equal to 1 and they reduce in the outer region. The values of empirical constants of Spalart-Allmaras turbulence model are given in Table 1.

Table 1. Empirical constants of Spalart-Allmaras turbulence model [12,13,17]

Constant	Value
c_{b1}	0.1355
σ	2/3
c_{b2}	0.622
κ	0.41
$c_{w1}=(c_{b1}/\kappa^2)+((1+c_{b2})/\sigma)$	3.2391
c_{w2}	0.3
c_{w3}	2
c_{v1}	7.1
c_{t1}	1
c_{t2}	2
c_{t3}	1.2
c_{t4}	0.5

2.4. Realizable k-ε Turbulence Model

In some turbulence models, two separate transport equations are used to determine the turbulence velocity scale and the length scale. These turbulence models are called two-equation models. The standard k-ε model proposed by Launder and Spalding is a two-equation model, which has been applied as an authentic model to numerous engineering applications [18]. Standard k-ε has a good performance, especially for flows where the Reynolds shear stresses are more significant [9]. Ability, economically-well and acceptable precision for a wide range of turbulent flows represents the validity of this model in the simulations of industrial flows. In this model, eddy viscosity is defined as follows [9,19,20,21]:

$$\mu_t = C_\mu \rho \frac{k^2}{\varepsilon} \tag{13}$$

Where k is turbulent kinetic energy per unit mass and ε is its rate of dissipation.

The standard k-ε model has been modified to improve its performance. The realizable k-ε model is a modified form of standard k-ε model. The transport equations for k and ε in this model is described by Eqs. (14) and (15) [9,20,21,22]:

$$\frac{\partial}{\partial t}(\rho k)+\frac{\partial}{\partial x_j}(\rho k u_j)=\frac{\partial}{\partial x_j}\left[\left(\mu+\frac{\mu_t}{\sigma_k}\right)\frac{\partial k}{\partial x_j}\right]+G_k+G_b-\rho\varepsilon-Y_M+S_k \tag{14}$$

And

$$\frac{\partial}{\partial t}(\rho \varepsilon)+\frac{\partial}{\partial x_j}(\rho \varepsilon u_j)=\frac{\partial}{\partial x_j}\left[\left(\mu+\frac{\mu_t}{\sigma_\varepsilon}\right)\frac{\partial \varepsilon}{\partial x_j}\right]+\rho c_1 S\varepsilon - \rho c_2 \frac{\varepsilon^2}{k+\sqrt{\nu\varepsilon}}+c_{1\varepsilon}\frac{\varepsilon}{k}c_{3\varepsilon}G_b+S \tag{15}$$

In these equations, σ_k and σ_ε are turbulent Prandtl numbers for k and ε, respectively. S_k and S_ε are source terms for k and ε that are defined by the user. Also, G_k represents the turbulent kinetic energy production [22]:

$$G_k = \mu_t S^2 \tag{16}$$

Where S is defined as modulus of mean rate-of-strain tensor [22]:

$$S = \sqrt{2S_{ij}S_{ij}}, \quad S_{ij} = \frac{1}{2}\left(\frac{\partial u_i}{\partial x_j} + \frac{\partial u_j}{\partial x_i}\right) \tag{17}$$

G_b denotes the generation of turbulent kinetic energy due to buoyancy and defined as [22]:

$$G_b = \beta g_i \frac{\mu_t}{\mathrm{Pr}_t}\frac{\partial T}{\partial x_i} \tag{18}$$

g_i is the component of gravitational vector in the ith direction. Also, the coefficient of thermal expansion is given by [22]:

$$\beta = -\frac{1}{\rho}\left(\frac{\partial \rho}{\partial T}\right)_p \tag{19}$$

Y_M represents contribution of fluctuating dilatation in compressible turbulence to the overall dissipation rate [22]:

$$Y_M = 2\rho\varepsilon M_t^2 \tag{20}$$

Here M_t is turbulent Mach number and defined as follows [22]:

$$M_t = \sqrt{\frac{k}{a^2}} \tag{21}$$

Where $a\left(=\sqrt{\gamma RT}\right)$ is the speed of sound. In addition,

$$c_1 = \max\left(0.43, \frac{\eta}{\eta+5}\right), \quad \eta = S\frac{k}{\varepsilon} \tag{22}$$

It may be noted that, C_μ in Eq. (13) is not constant, but rather, it is defined as [20,21]:

$$C_\mu = \frac{1}{A_0 + A_s U^* \frac{k}{\varepsilon}} \tag{23}$$

Where A_0 is a constant and A_s and U^* are determined based on the Eqs. (24) and (25):

$$A_s = \sqrt{6}\cos(\phi),$$
$$\phi = \frac{1}{3}\arccos\left(\sqrt{6}W\right),$$
$$W = \frac{S_{ij}S_{jk}S_{ki}}{\tilde{S}^3}, \quad (24)$$
$$\tilde{S} = \sqrt{S_{ij}S_{ij}}$$

$$U^* = \sqrt{S_{ij}S_{ij} + \Omega_{ij}\Omega_{ij}} \quad (25)$$

Empirical constants of realizable k-ε model are given in Table 2.

Table 2. Empirical constants of realizable k-ε turbulence model [20,21]

Constant	Value
A_0	4.04
$c_{1\varepsilon}$	1.44
$c_{3\varepsilon}$	-0.33
c_2	1.9
σ_k	1.0
σ_ε	1.2

2.5. k-ω Shear Stress Transport (SST) Turbulence Model

The standard k-ω model is based on Wilcox k-ω model, which incorporates modifications for low Reynolds number effects and compressibility. The modified standard k-ω model is known as k-ω SST developed by Menter [23]. The k-ω SST model is a combination of k-ω model (in the inner boundary layer) and k-ε model (outside of the boundary layer). Therefore, this model can be used in a wide range of engineering applications, which involve high Reynolds number regions far from the wall and low Reynolds number regions near to the wall). Researchers believe that k-ω SST presents a very good behavior in problems with flow separation and adverse pressure gradient. The transport equations of turbulence kinetic energy k and turbulence frequency ω are given as follows [23]:

$$\frac{\partial}{\partial t}(\rho k) + \frac{\partial}{\partial x_j}(\rho k u_j) = \tau'_{ij}\frac{\partial u_i}{\partial x_j} - \beta^*\rho\omega k + \frac{\partial}{\partial x_j}\left[(\mu + \sigma_k\mu_t)\frac{\partial k}{\partial x_j}\right] \quad (26)$$

$$\frac{\partial}{\partial t}(\rho\omega) + \frac{\partial}{\partial x_j}(\rho\omega u_j) = \frac{\gamma}{\nu_t}\tau'_{ij}\frac{\partial u_i}{\partial x_j} - \beta\rho\omega^2 + \frac{\partial}{\partial x_j}\left[(\mu + \sigma_\omega\mu_t)\frac{\partial \omega}{\partial x_j}\right] + 2(1-F_1)\frac{\rho\sigma_{\omega 2}}{\omega}\frac{\partial k}{\partial x_j}\frac{\partial \omega}{\partial x_j} \quad (27)$$

Where $\nu_t=\mu_t/\rho$ is turbulence kinematic viscosity and $\beta^*=\varepsilon/k\omega=0.09$. The turbulence stress tensor τ'_{ij} is set according to Eq. (6).

In the k-ω SST model, the eddy viscosity is estimated as $\mu_t=\rho a_1 k/\max(a_1\omega,\Omega F_2)$ where $\Omega=\sqrt{2\Omega_{ij}\Omega_{ij}}$ is the vorticity magnitude and a_1=0.31. The function F_2 is determined according to Eq. (28) [23,24]:

$$F_2=\tanh\left\{\left[\max\left(\frac{2\sqrt{k}}{\beta^*\omega y},\frac{500\nu}{y^2\omega}\right)\right]^2\right\} \tag{28}$$

Here, y is the distance of field point to the nearest surface.

The coefficients β, γ, σ_k and σ_ω are defined as functions of the coefficients related to k-ω and k-ε turbulence models [23,24]:

$$\begin{aligned}\beta&=F_1\beta_1+(1-F_1)\beta_2,\\ \gamma&=F_1\gamma_1+(1-F_1)\gamma_2,\\ \sigma_k&=F_1\sigma_{k1}+(1-F_1)\sigma_{k2},\\ \sigma_\omega&=F_1\sigma_{\omega1}+(1-F_1)\sigma_{\omega2}\end{aligned} \tag{29}$$

The function F_1 is given as [24]:

$$\begin{aligned}F_1&=\tanh\left((\min[\arg])^4\right),\\ \arg&=\max\left(\frac{\sqrt{k}}{\beta^*\omega y},\frac{500\nu}{y^2\omega}\right),\frac{4\rho\sigma_{\omega2}k}{CD_{k\omega}y^2}\end{aligned} \tag{30}$$

Where,

$$CD_{k\omega}=\max\left(\frac{2\rho\sigma_{\omega2}}{\omega}\frac{\partial k}{\partial x_j}\frac{\partial\omega}{\partial x_j},10^{-20}\right) \tag{31}$$

Finally, the experimental coefficients for the k-ω SST model are given in Table 3.

Table 3. Empirical constants of k-ω SST turbulence model [24]

Constant	Value
β_1	0.075
β_2	0.0828
σ_{k1}	0.85
σ_{k2}	1.0
$\sigma_{\omega1}$	0.5
$\sigma_{\omega2}$	0.856
κ	0.41
$\gamma_1=\frac{\beta_1}{\beta^*}-\frac{\sigma_{\omega1}\kappa^2}{\sqrt{\beta^*}}$	0.5532
$\gamma_2=\frac{\beta_2}{\beta^*}-\frac{\sigma_{\omega2}\kappa^2}{\sqrt{\beta^*}}$	0.4404

3. SOLUTION METHOD AND COMPUTATIONAL DOMAIN

In the present work, in order to validate the current simulation results, the Reynolds number is set equal to 3×10^6 being identical to that considered in the experiments carried out by Abbott and von Doenhoff [25]. Free stream temperature is set the equal to the ambient temperature (T=300 K) for which the density and viscosity are equal respectively to ρ=1.1761 kg.m^{-3} and μ=1.8536×10^{-5} kg.m^{-1}s^{-1}. The open-source software package OpenFOAM is used and calculations are performed for attack angles varying from -12º to 20º.

In OpenFOAM solver, the spatial discretization of the equations is achieved using finite volume method (FVM) on block structured meshes with Gaussian integration and linear interpolation. Among available techniques, temporal discretization is obtained with Euler blended Crank-Nicolson time stepping scheme (with blending factor of 0.5) to improve the stability. The velocity-pressure coupling is performed using the PISO (Pressure Implicit with Splitting of Operators) algorithm given in Figure 1.

For solution of the momentum equations, the preconditioned bi-conjugate gradient (PBiCG) with diagonal based incomplete LU (DILU) preconditioner is employed. Furthermore, the pressure equation is solved using a geometric agglomerated algebraic multigrid (GAMG) solver with a Gauss-Seidel type smoother. The simulations were run until the residual of the pressure and velocities were less than 10^{-8} and 10^{-6}, respectively.

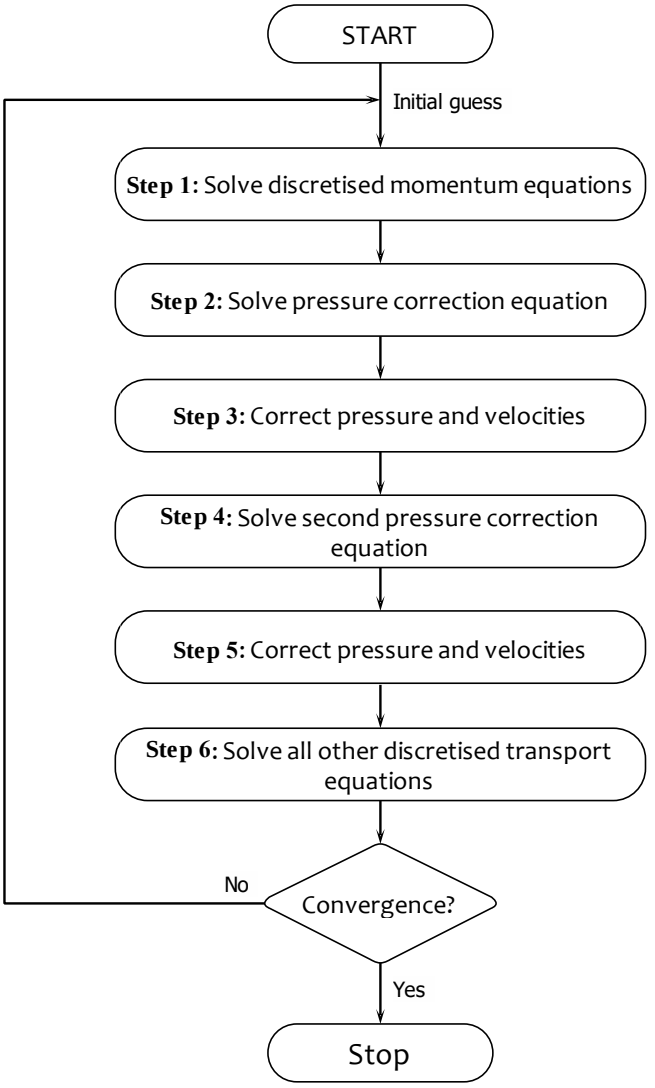

Figure 1. The PISO algorithm [9]

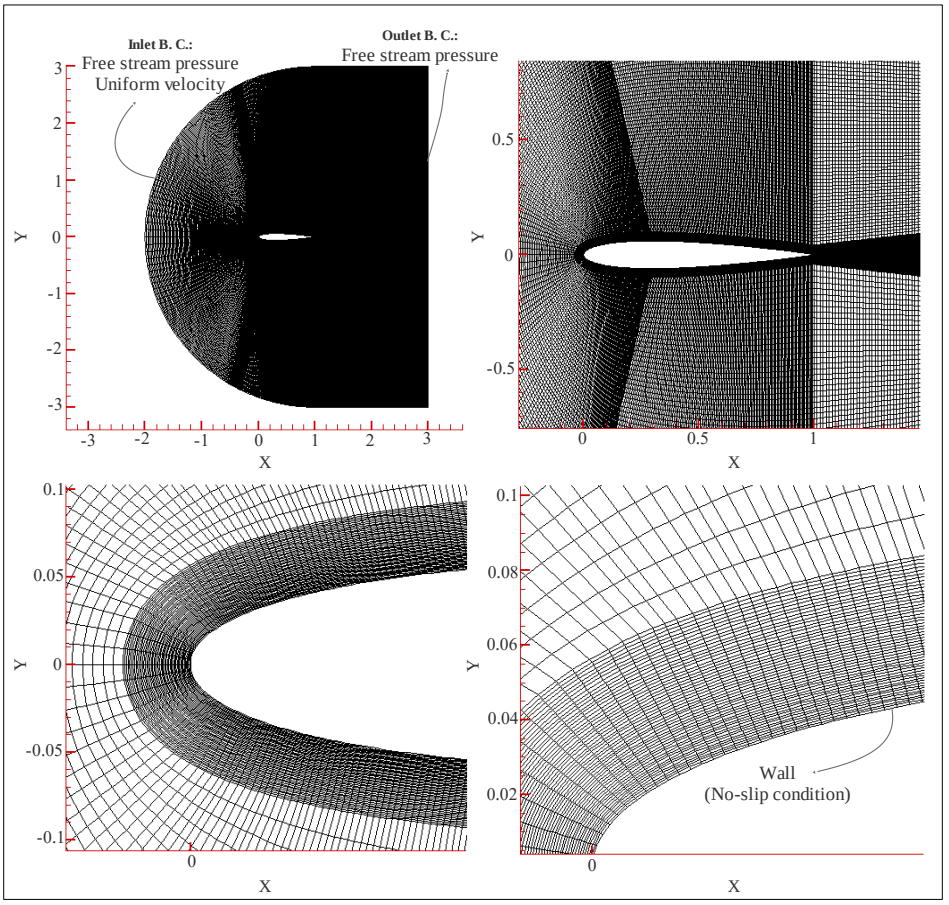

Figure 2. Schematic of structured grid around NACA0012 airfoil

A typical structured quadratic (rectangular cells) grid used for the analyses is shown in Figure 2. Gambit software is used to model the airfoil (with chord length of 1 meter) and create the C-type computational domain. The free stream pressure is used for the pressure at the inlet and outlet boundaries. A uniform velocity is prescribed at the inlet. Furthermore, the no-slip condition is used on the airfoil wall boundary. The regions with strong gradients of flow variables (like the region near to airfoil), a finer grid is used. The distance of the airfoil surface from the center of nearest computational cell is about 10-5 leading to the maximum y+ of 0.195.

One of the main steps in any CFD simulation is to investigate the effect of mesh size on the solution results. Indeed, the accuracy of numerical solution is dependent on the number of nodes. Using additional nodes causes the increase of required computer memory and computational time. In this study, the grid independent test was performed with four different number of grid cells as given in Table 4. The results associated with the lift coefficient at attack angel of 4º using Spalart-Allmaras turbulence model were assessed. It was observed that the lift coefficient for the last two number of grid cells was almost the same. Hence, using the number of 150,000 cells for current problem was found to be appropriate.

Table 4. Grid independence test results

Cells No.	Lift coefficient	Error (%)
60000	0.403385	6.19
100000	0.417453	2.92
150000	**0.426572**	**0.8**
240000	0.426697	0.77

4. RESULTS AND DISCUSSION

The subsonic turbulent flow (Mach = 0.13) around NACA0012 airfoil at different angles of attack (from -12º to 20º) is simulated using three different turbulence models and the obtained results are compared with the available experimental data. The variations of lift coefficient C_L and drag coefficient C_D versus the angle of attack are given in Figures 3 and 4, respectively.

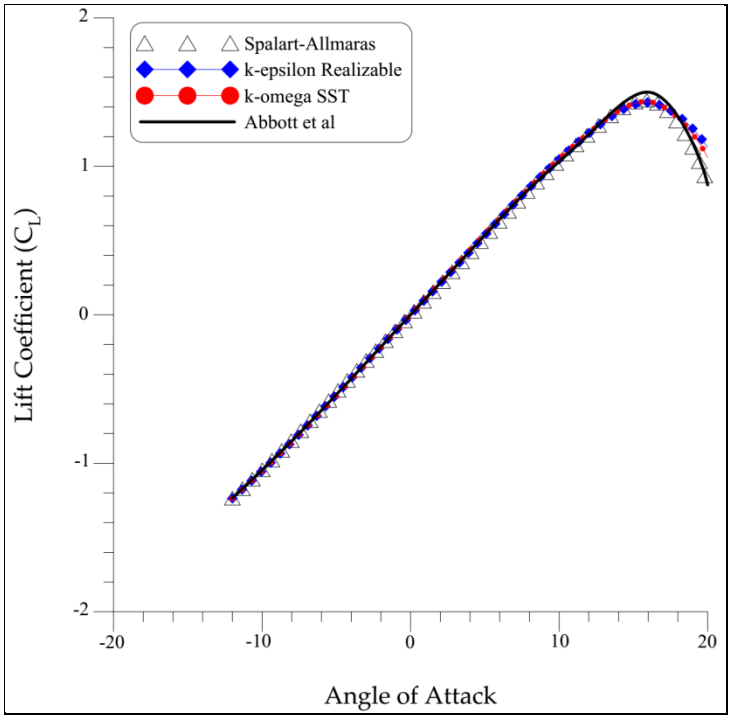

Figure 3. Comparison of lift coefficient obtained by experimental results [25] and three different turbulence models

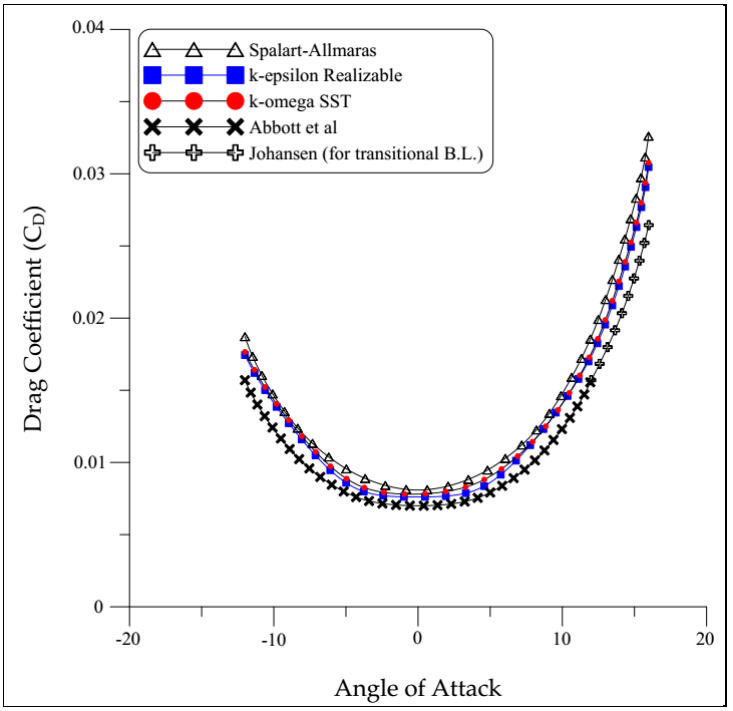

Figure 4. Comparison of drag coefficient obtained by experimental results [3,25] and three different turbulence models

Figure 3 demonstrates that for angles of attack from -12º to 12º, the lift coefficient C_L increases linearly with angle of attack. In this range of attack angle the flow around the airfoil is continuous without separation. Therefore, the results obtained from all the three turbulence models are in good agreement with the corresponding experimental data. As the attack angle is increased to about 15º, flow separation and consequently the so-called stall condition would occur. At this angle that is recognized as critical angle of attack, the maximum C_L is obtained. From the critical angle of attack to 20º, C_L is decreased. Within this range, the Spalart-Allmaras model gives rise to higher accuracy than the other two turbulence models. The maximum error is associated with the angle of attack of 16º and is equal to 3.67%.

According to Figure 4, the predicted drag coefficients C_D at all the angles of attack considered, are slightly higher than the corresponding experimental data. This result may be expected because in reality in front section of the airfoil the flow is laminar rather than turbulent. However, many turbulence models consider the boundary layer along the entire length of airfoil to be turbulent and hence they are not able to capture the transition from laminar to turbulent. The turbulent boundary layer transfers more energy compared to the laminar boundary layer and its drag coefficient C_D is higher. In fact, utilization of a fully turbulent model for analysis of the entire flow field may give rise to erroneous results. Therefore, true and reliable evaluation of the performance of a turbulence model requires the experimental data obtained from fully turbulent boundary layer. It may be noted that, the turbulence models could be consistently used for prediction of C_L, due to the fact that it is less sensitive to the transition region. However, for calculation of C_D, the above considerations should be well taken care of.

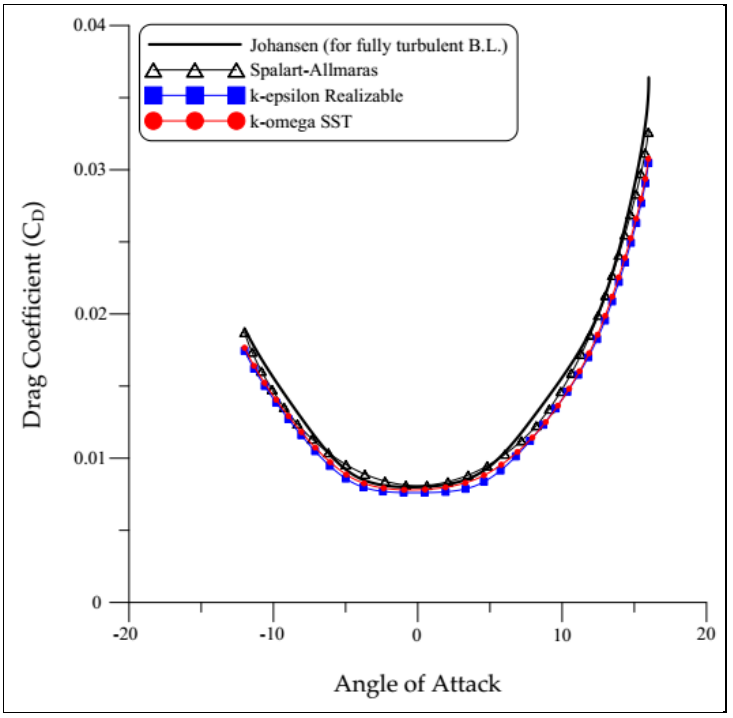

Figure 5. Comparison of drag coefficient obtained by experimental results [3] and three different turbulence models

Johansen has reported the experimental data of C_D for NACA0012 airfoil obtained at $Re=3\times10^6$ pertaining to turbulent boundary layer around the airfoil [3]. Figure 5 shows the comparison of the predicted C_D for different angles of attack with the corresponding experimental data associated with the fully turbulent boundary layer. As it can be seen, for all the turbulence models, the current predicted C_D values are in good agreement with the experimental results of turbulent boundary layer. The most accurate model is Spalart-Allmaras model. The k-ω SST model and the realizable k-ε model are placed in the second and third places from the accuracy view point, respectively.

In order to predict the aerodynamic coefficients more accurately, the transition region effects should be accounted for. This would require the determination of exact position of transition point. Transition state could be thought of as a bridging gap between fully laminar upstream and fully turbulent downstream flow. Therefore, either the external flow over a solid surface or the internal flow through a channel should inevitably pass through the transition region, starting from a laminar region, before reaching a fully turbulent region. Any error due to inaccurate modeling of the transition region or due to totally ignoring this region could cause the flow quantities to be over-/under-predicted. The latter (i.e., ignoring the transition region) has become a common practice by the researchers in both numerical analyses and experiments. This error, more or less is dependent on the commencement of transition region and its extent. Disregarding the onset of transition region and its length and most importantly the main parameters affecting this region would cause any turbulence model to fail in accurate computation of physical parameters (e.g., drag coefficient) for even the simple problem of flow over a flat plate.

Boutilier empirically investigated the incompressible flow over a NACA0018 airfoil at $Re=1\times10^5$ [26]. He expressed that in downstream of the transition position, rapid pressure recovery occurs. Additionally, at approximate position of the transition point, the maximum displacement thickness of boundary layer was observed. He also demonstrated that the momentum thickness of boundary layer at the upstream of the transition point is fairly constant, but at the immediate downstream of the transition position it begins to increase suddenly with a positive gradient. Consequently, he detected the pressure recovery, the displacement thickness and the momentum thickness as the effective and useful parameters in determination of the transition point.

In the present article, for more accurate calculation of the flow features, the method suggested by Silisteanu and Botez is used [27]. In this method, the computational domain is split into two distinct regions of turbulent and laminar. The disadvantages of this approach are to guess the location of the transition point and the requirement for generation of new mesh as the transition point changes. The process of determination of transition point x_{tr} is briefly described below. First, the position of transition point is guessed and the computational domain is split into laminar and turbulent regions using a vertical line. The problem is solved in OpenFOAM by considering the laminar flow equations on the left hand side and turbulent flow equations on the right hand side of the vertical line. If the obtained C_D value is greater (smaller) than the experimental counterpart, the turbulent region has been considered larger (smaller) than its real magnitude. Then, the location of transition point needs to be corrected and problem solution should be repeated. Finally, using linear interpolation, the proper location of transition point is determined. The results obtained using this method for $Re=1\times10^6$ to $Re=5\times10^6$ to at 0º angle of attack is depicted in Figure 6. First, C_D is computed for fully turbulent boundary layer using Spalart-Allmaras model and compared to the experimental results published by McCroskey et al. [4]. Then the computational domain is split into two regions of laminar and turbulent ones and the transitional boundary layer is solved. The computational results for fully turbulent boundary layer are in acceptable agreement with the experimental data. The maximum difference between the computed drag coefficient and its empirical counterpart for the case of fully turbulent boundary layer is about 2.671% at $Re=5\times10^6$. In addition, the computational results for the case of transitional boundary layer are in very good agreement with the empirical data where the maximum error at $Re=3\times10^6$ is observed to be equal to 0.955%. It can also be observed from Figure 5 that C_D decreases as the Reynolds number is increased. In the case of fully turbulent boundary layer, the reduction in C_D with Reynolds number is more intensive than for the case of transitional boundary layer. It is worth noting that in 0º angle of attack, the transition point can be specified more easily because it is located on a common vertical line on both the upper and lower surfaces of airfoil due to the symmetrical nature of NACA0012 airfoil. But in non-zero angles of attack, this process is more complex due to the asymmetry of flow on the upper and lower surfaces of the airfoil.

Figures 7-10 show the contours of static pressure at attack angles of 0º, 4º, 8º and 16º, respectively using Spalart-Allmaras model. As can be seen at attack angle of 0º, the pressure distribution on the upper and lower surfaces of the airfoil is the same, but with increasing angle of attack, the pressure on the lower surface of airfoil increases. This leads to the generation of an upward force perpendicular to the main flow direction (i.e., the lift force). On the other hand, those components of the pressure parallel to free stream operate as opposing force (i.e., the drag force).

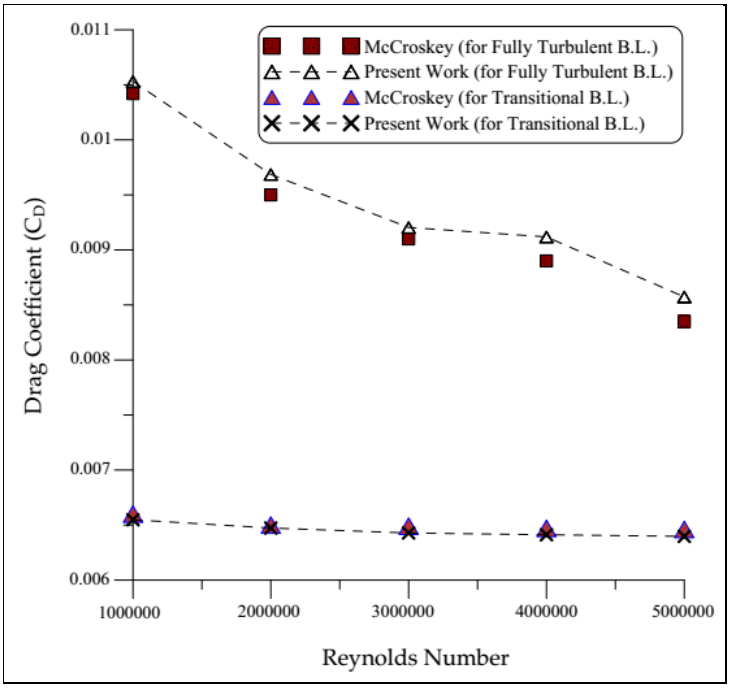

Figure 6. Comparison of simulation results with experimental data presented with McCroskey et al. [4] for transitional and fully turbulent boundary layers

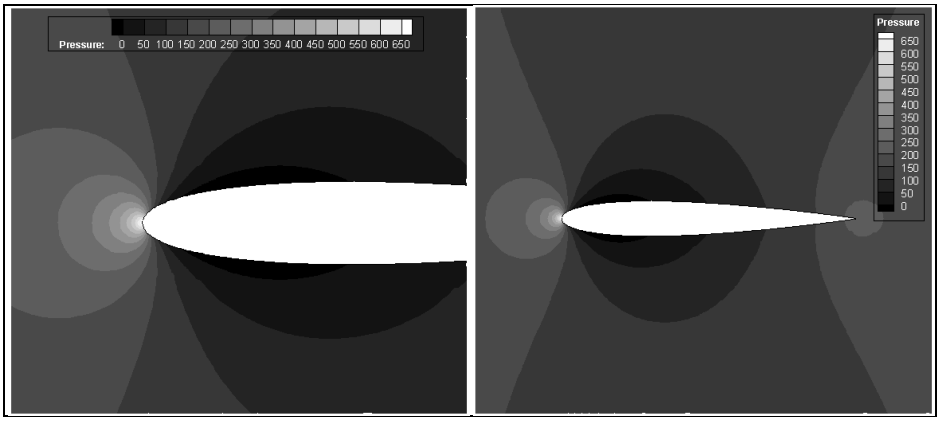

Figure 7. Static pressure distribution in 0º angle of attack which is obtained by Spalart-Allmaras turbulence model

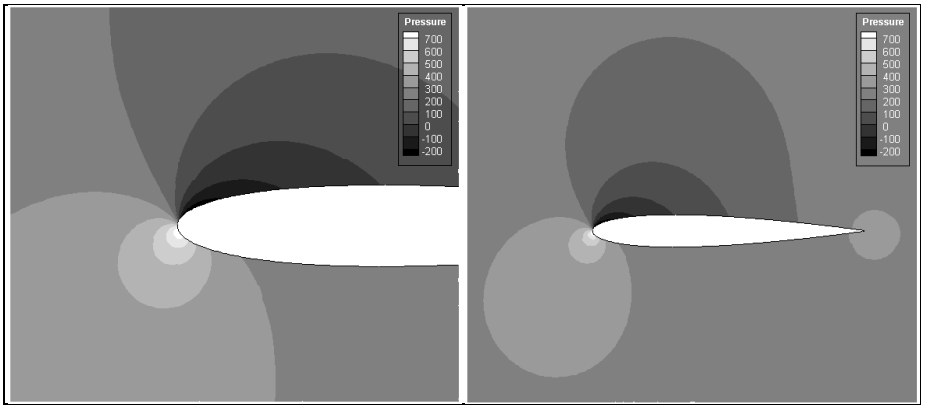

Figure 8. Static pressure distribution in 4º angle of attack which is obtained by Spalart-Allmaras turbulence model

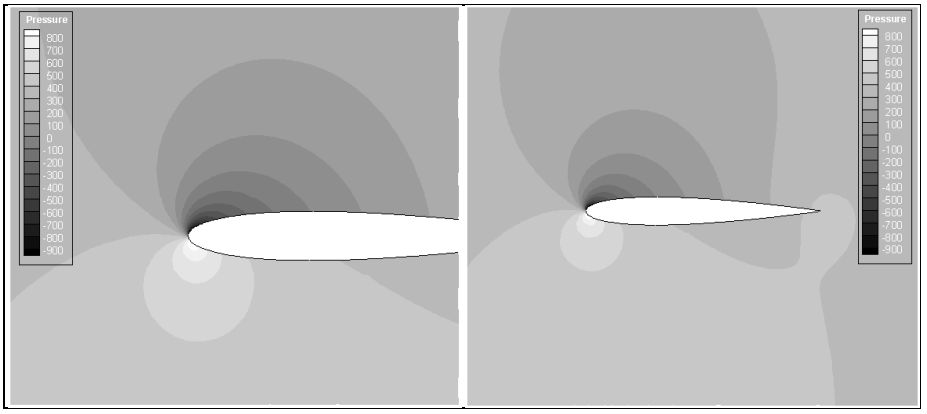

Figure 9. Static pressure distribution in 8º angle of attack which is obtained by Spalart-Allmaras turbulence model

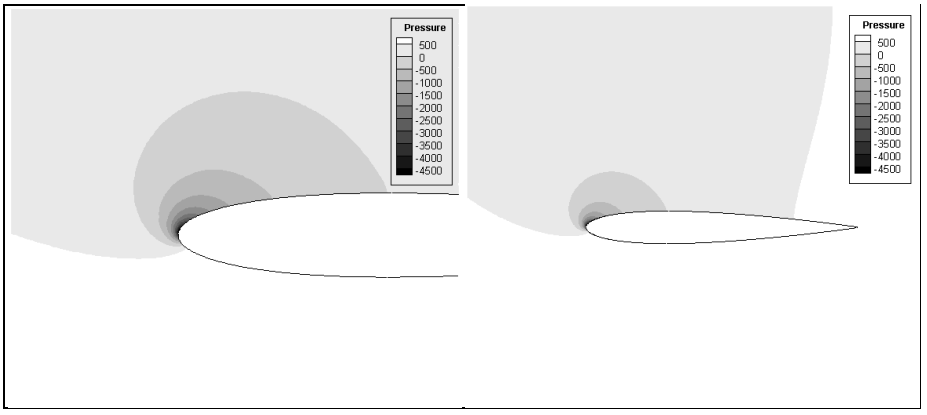

Figure 10. Static pressure distribution in 16º angle of attack which is obtained by Spalart-Allmaras turbulence model

The velocity distribution over the airfoil at 4º and 8º angles of attack along with the streamlines is shown in Figures 11 and 12, respectively. According to these figures, streamlines in the region over the upper surface of the airfoil are closer together implying that the velocity magnitudes are larger there than those in the region under the lower surface of the airfoil. These results are consistent with the results of static pressure contours shown in Figures 8 and 9. With increasing the angle of attack, the velocity on the upper surface is increased (streamlines become closer together) and the velocity difference between the upper and lower surfaces of airfoil becomes greater. On the other hand, with increasing the angle of attack, the stagnation point on the leading edge of the airfoil is displaced towards the trailing edge of airfoil.

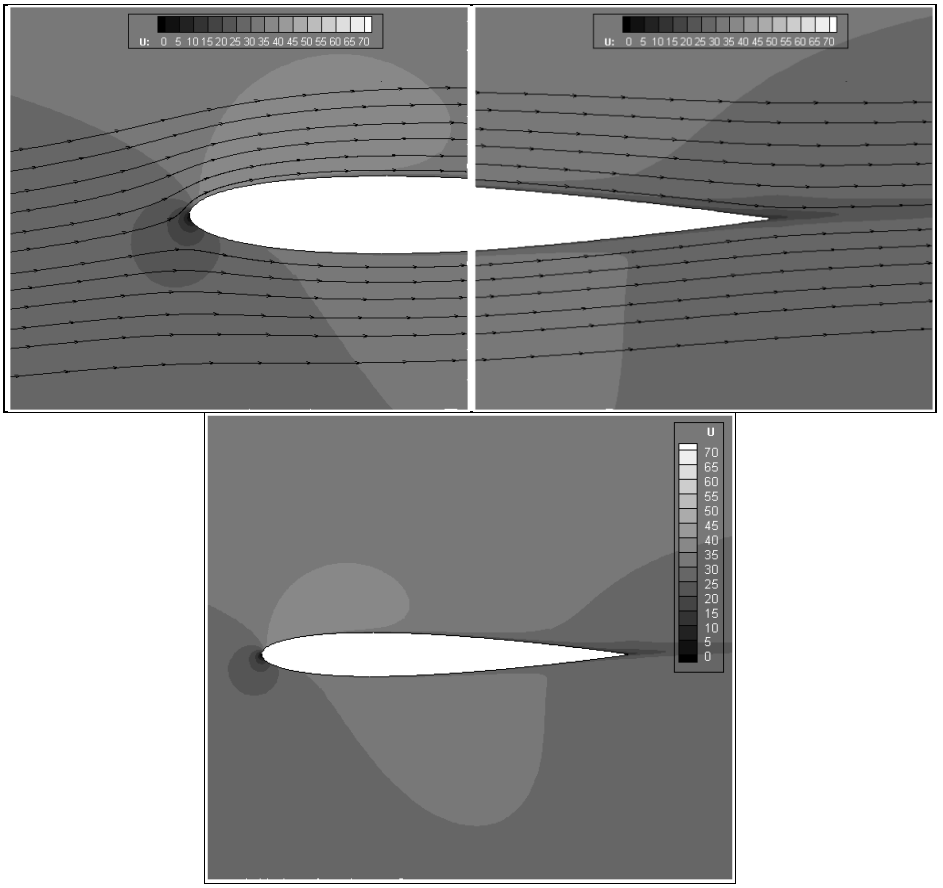

Figure 11. Velocity distribution in 4º angle of attack which is obtained by Spalart-Allmaras turbulence model

5. CONCLUSION

In this paper, the accuracy of three turbulence models of Spalart-Allmaras, realizable k-ε and k-ω SST in the simulation of flow over NACA0012 airfoil is investigated using OpenFOAM. In addition, for accurate investigation of the simulation results, the transition and turbulent regions are treated separately, which have remarkable importance in CFD simulations. The results from

these analyses express that:

- Among the three investigated turbulence models, Spalart-Allmaras model, which is a one-equation model, has highest accuracy. As explained in the article, this model is designed for aerospace applications and offers fine results for boundary layers being exposed to the inverse pressure gradient.

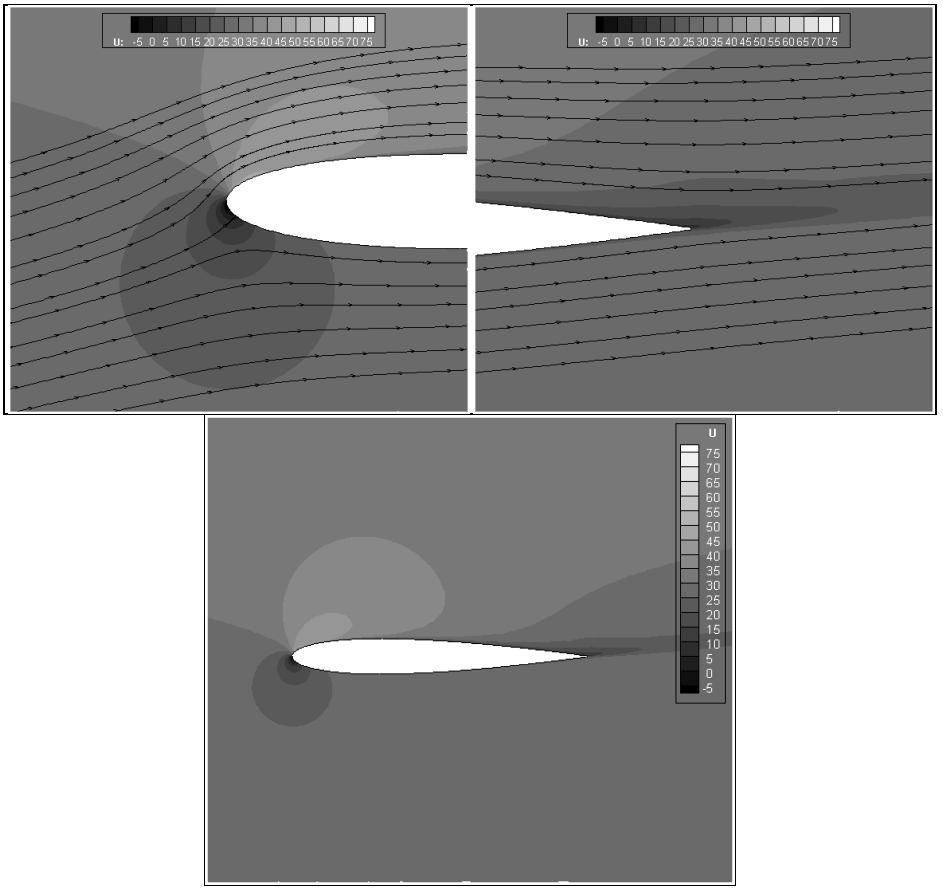

Figure 12. Velocity distribution in 8º angle of attack which is obtained by Spalart-Allmaras turbulence model

- The drag coefficient predicted by the turbulence models was greater than that obtained from the experiments. This result might have been expected because in actual conditions, the flow over part of the airfoil is laminar and over part of it becomes turbulent, but all turbulence models use the assumption of fully turbulent flow all around the airfoil. Since the energy transfer in turbulent boundary layer is higher than the laminar boundary layer, the predicted C_D by turbulence models is also higher than the actual conditions. Acceptable agreement between the simulation results and the experimental data was observed.

- To make more realistic the flow conditions around the airfoil in simulation, the proper location of transition point in which flow regime is converted from laminar to turbulent is determined and computational grid is split into two regions of laminar and turbulent flows. The

results obtained by this method had great consistency with experimental data. Transition from the fully laminar flow to fully turbulent flow is one of the phenomena, which has been less considered in experimental tests and numerical analyses. Therefore, it is recommended to consider transition region in both the theoretical and empirical studies to gain more realistic results.

Acknowledgements / Teşekkür

We would like to thank Dr. Javad Aminian, Faculty member of Mechanical and Energy Engineering at Shahid Beheshti University, for his genuine support to do this research work.

NOMENCLATURE

a	Speed of sound
C_D	Drag coefficient
C_L	Lift coefficient
c_p	Heat capacity at constant pressure
d	Distance to the closest wall
d_t	Distance of a point in the flow field to trip
E	Total energy
f_{v1}	Damping function
G_b	Generation of turbulent kinetic energy from buoyancy
G_k	Turbulent kinetic energy production due to average velocity gradients
k	Turbulent kinetic energy per unit mass
M_t	Turbulent Mach number
p	Static pressure
Pr_t	Turbulent Prandtl number
Re	Reynolds number
S	Modulus of mean rate-of-strain tensor
S_{ij}	Strain rate tensor
S_{M_j}	Total effect of body forces per unit volume per unit mass
T	Temperature
u_j	Velocity component
Y_M	Contribution of fluctuating dilatation to overall dissipation rate

REFERENCES / KAYNAKLAR

[1] Saniei Nejad M., Mani M., (2014) Numerical comparison between physics of transitional flow and full turbulent flow around classical airfoil of NACA0012 at subsonic and transonic regimes, *Journal of Fluid Mechanics and Aerodynamics* 2, 63–87. (In Persian)

[2] Bacha W.A., Ghaly W.S., (2006) Drag prediction in transitional flow over two-dimensional airfoils, *44th AIAA AeroSpace Sciences Meeting and Exhibit*, Reno, Nevada, USA. doi: 10.2514/6.2006-248.

[3] Johansen J., (1997) Prediction of laminar/turbulent transition in airfoil flows, *RisØ National Laboratory*, Roskilde, Denmark.

[4] McCroskey W.J., et al., (1987) A critical assessment of wind tunnel results for the NACA0012 airfoil, *U.S. Army Aviation Research and Technology Activity: Nasa Technical Memorandum* 42, 285–330.

[5] Maksymiuk C.M., Pulliam T.H., (1987) Viscous transonic airfoil workshop results using ARC2D, *25th AIAA Aerospace Sciences Meeting and Exhibit*, 12–15 January 1987, Reno, Nevada, USA. doi: 10.2514/6.1987-415.

[6] Arias O., Falcinelli O., Fico N., Elaskar S., (2007) Finite volume simulation of a flow over a NACA0012 using Jameson, Maccormack, Shu and Tvd Esquemes, *Mecanica Computational* 26, 3097–3116.

[7] Barter G.E., (2008) Shock capturing with PDE-based artificial viscosity for an adaptive, higher-order discontinuous Galerkin finite element method, PhD Thesis, *Massachusetts Institute of Technology*, USA.

[8] Batchelor G.K., (1967) An introduction to fluid dynamics. *Cambridge University Press*, Cambridge, UK.

[9] Versteeg H.K., Malalasekera W., (2007) An introduction to computational fluid dynamics: The finite volume method, 2nd ed., *Pearson Education Limited*, ISBN: 978-0-13-127498-3.

[10] Saniei Nejad M., (2009) Fundamentals of turbulent flows and turbulence modeling, *Danesh Negar Press*, Tehran, Iran. (In Persian)

[11] Schmitt F.G., (2007) About boussinesq's turbulent viscosity hypothesis: Historical remarks and a direct evaluation of its validity, *Comptes Rendus Mécanique* 335, 617–627. doi: 10.1016/j.crme.2007.08.004.

[12] Deck S., Duveau P., Espiney P., Guillen P., (2002) Development and application of Spalart–Allmaras one equation turbulence model to three-dimensional supersonic complex configurations, *Aerospace Science and Technology* 6, 171–183. doi: 10.1016/S1270-9638(02)01148-3.

[13] Spalart P.R., Allmaras S.R., (1992) A one-equation turbulence model for aerodynamic flows, *AIAA Paper*, No. 92–0439. doi: 10.2514/6.1992-439.

[14] Deck S., Hallard R., (2001) Numerical simulation of separated flows in nozzles, *37 eme Colloque d'Aerodynamique Appliquee*, 28-30 March 2001, Arcachon, France.

[15] Gacherieu C., Weber C., (1998) Assessment of algebraic and one-equation turbulence models for the transonic turbulent flow around a full aircraft configuration, *AIAA Paper*, No. A98–32457. doi: 10.2514/6.1998-2737.

[16] Rogers S.E., Roth K., Nash S.M., Baker M.D., Slotnick J.P., Whitlock M., Cao H.V., (2000) Advances in overset CFD processes applied to subsonic high-lift aircraft, *AIAA Paper*, No. A00–39874. doi: 10.2514/6.2000-4216.

[17] Wilcox D.C., (1993) Turbulence modeling for CFD. *DCW Industries*, California, USA. ISBN: 0-9636051-0-0.

[18] Launder B.E., Spalding D.B., (1974) The numerical computation of turbulent flows, *Computer Methods in Applied Mechanics and Engineering* 3, 269–289. doi: 10.1016/0045-7825(74)90029-2.

[19] Hassanzadeh A., Saadat Bakhsh M., Dadvand A., (2014) Numerical study of the effect of wall injection on the cavitation phenomenon in diesel injector, *Engineering Applications of Computational Fluid Mechanics* 8, 562–573. doi: 10.1080/19942060.2014.11083307.

[20] Marzouk O.A., Huckaby E.D., (2010) Simulation of a Swirling Gas-Particle Flow Using Different k-epsilon Models and Particle-Parcel Relationships, *Engineering Letters*, 18:1, EL_18_1_07.

[21] Shih T.H., Liou W.W., Shabbir A., Yang Z., Zhu J., (1995) A new k-ε eddy-viscosity model for high Reynolds number turbulent flows, *Computers & Fluids* 24, 227–238. doi: 10.1016/0045-7930(94)00032-T.

[22] Yeh C.L., (2012) Numerical investigation of the heat transfer and fluid flow in a carbon monoxide boiler, *International Journal of Heat and Mass Transfer* 55, 3601–3617. doi: 10.1016/j.ijheatmasstransfer.2012.02.073.

[23] Menter F.R., (1994) Two-equation eddy-viscosity turbulence models for engineering applications, *AIAA Journal* 32, 1598–1605. doi: 10.2514/3.12149.

[24] Eca L., Hoekstra M., (2011) Numerical aspects of including wall roughness effects in the k-ω SST eddy-viscosity turbulence model, *Computers & Fluids* 40, 299–314. doi: 10.1016/j.compfluid.2010.09.035.

[25] Abbott I.H., von Doenhoff A.E., (1959) Theory of wing section. *Dover Publishing*, New York, USA.

[26] Boutilier M.S.H., (2011) Experimental investigation of transition over a NACA0018 airfoil at a low Reynolds number, PhD Thesis, *University of Waterloo*, Ontario, Canada.

[27] Silisteanu P.D., Botez R.M., (2010) Transition flow occurrence estimation: A new method. *Journal of Aircraft* 47, 703–708. doi: 10.2514/1.44698.